Mesoscopic physics in vapor-phase atomic systems: Collision-shift gradients and the 0-0 hyperfine transition

Andrew Hudson and James Camparo
Photonics Technology Department, Physical Sciences Laboratories, The Aerospace Corporation, P.O. Box 92957, Los Angeles, California 90009, USA

(Received 23 June 2018; published 19 October 2018)

Vapor-phase atomic clocks and atomic magnetometers are achieving levels of stability and measurement precision today that would have been considered unrealistic in the not too distant past. To make further progress, researchers will need a more detailed understanding of vapor-phase atomic physics, in particular, the manner in which *mesoscopic* variations of atomic perturbations map onto the observed resonant phenomena: length scales larger than that of homogeneous quantum dynamics, where atoms within some localized region of the vapor all experience the same optical and microwave fields and collisional perturbations; but smaller than that of the vapor as a whole, where the atomic system is described in terms of (for example) vapor pressure, heat content, and optical depth. In this paper, we discuss the issue of mesoscopic physics as it manifests itself in vapor-phase collision-shift gradients affecting the 0-0 hyperfine transition of ^{87}Rb. We show that these gradients not only produce increased line broadening but lead to lineshape asymmetry and an increased sensitivity of the observed resonance to power-broadening. We develop a statistical theory describing the experimental results, and through that theory we show that mesoscopic atomic physics encompasses a broader class of phenomena than that described by the circumscribed term "inhomogeneous broadening."

DOI: 10.1103/PhysRevA.98.042510

I. INTRODUCTION

At the microscopic level of atomic dynamics (i.e., spatial scales where all atoms experience the same Hamiltonian) perturbations affecting the hyperfine transition of alkali-metal atoms in the vapor-phase are fairly well understood. There is a well-founded understanding of the ac-Stark shift [1,2]; researchers have a good grasp of the physics of spin-exchange [3,4] (though we can still be surprised by nonintuitive consequences of the interaction [5,6]), and we know well the effect of weak and strong magnetic fields on the ground-state hyperfine structure [7,8]. In particular, at the microscopic scale it is relatively straightforward to set up the density matrix equations for a multilevel alkali atom, include all the perturbations acting on the atom, and solve those equations (numerically if necessary) to predict the atom's behavior under any arbitrary set of conditions.

Notwithstanding this good understanding of microscopic vapor-phase atomic dynamics, evidence has been mounting for another scale of physics that contributes to the 0-0 hyperfine transition lineshape that is not so well understood. For lack of a better term, we refer to this vapor-phase regime of spatial dimensions as the *mesoscopic* scale. By mesoscopic, we mean spatial scales larger than the atoms' microscopic quantum dynamics but smaller than the scale of the vapor as a whole (e.g., vapor pressure, vapor heat content, vapor optical depth). This scale comes into atomic physics because in many vapor-phase systems the atoms are spatially confined by buffer-gas collisions on time intervals long compared to a perturbation's effective timescale (e.g., the Rabi period for an alkali atom's 0-0 hyperfine transition). Thus, the atoms in the vapor's signal volume experience *local* perturbations, which combine nonlinearly to produce the vapor's overall (i.e., observed) atomic signal. Some examples of important mesoscopic phenomena related to the 0-0 hyperfine transition in alkali atoms that have been discovered to date include: the position-shift effect [9], the inhomogeneous light shift [10], and the effect of inhomogeneous-field saturation broadening [11].

Clearly, what we are describing as mesoscopic physics has strong ties to processes related to traditional inhomogeneous broadening, as exemplified by the inhomogeneous light shift and position shift noted above. Consequently, one might legitimately question our insistence on the mesoscopic label, when inhomogeneous broadening might suffice. The point to note, however, is that when discussing inhomogeneous broadening one is primarily restricting attention to spatial variations of the atom's resonant frequency. Here, we are concerned with a broader class of phenomena. For example, in the case of inhomogeneous-field saturation broadening noted above there need be no variation of the atoms' resonant frequency from one spatial region to another. Instead, changes in the observed lineshape arise because different regions of the vapor come into saturation at different power levels due to the field-amplitude's modal distribution in a cavity. The effect is present without any variation of the atom's resonant frequency, and describing this as an effect of inhomogeneous broadening would be misleading. We will have more to say about the inhomogeneous-broadening/mesoscopic-physics distinction in our conclusions.

Several years ago, Oreto *et al.* [12] clarified what is arguably one of the more important manifestations of

mesoscopic physics [13]. Specifically, for isobaric vapor-phase systems temperature gradients result in density gradients, and buffer-gas density gradients result in spatially-varying collision shifts of atomic resonance lines. To illustrate, consider a fractional-frequency collision shift of the ^{87}Rb 0-0 hyperfine resonance, $\delta y_{\rm col}$ (i.e., $\delta y = \delta\nu_{\rm hfs}/\nu_{\rm hfs}$). This collision shift scales like $[{\rm BG}]\bar{v}\lambda_{\rm col}$, where [BG] is the number density of buffer-gas molecules in the vapor, $\bar{v}$ is the mean collision speed, and $\lambda_{\rm col}$ is a collision-shift coefficient. Under isobaric conditions (and considering two regions A and B at slightly different temperatures $\Theta_{\rm J}$) the ratio of 0-0 resonance shifts in those two regions becomes [14]

$$\frac{\delta y_{\rm col}(A)}{\delta y_{\rm col}(B)} \cong \frac{\Theta_B}{\Theta_A} \Rightarrow \Delta y \equiv [\delta y_{\rm col}(B) - \delta y_{\rm col}(A)] = \delta y_{\rm col}(B)\left(1 - \frac{\Theta_B}{\Theta_A}\right). \quad (1)$$

For an ^{87}Rb vapor-phase system at 50 °C, confined with a typical buffer gas like N_2 at a 10 torr buffer-gas pressure, $\delta y_{\rm col} \sim 10^{-6}$ [15]. Consequently, to keep Δy variations across the vapor's signal volume to less than 10^{-14} (a required stability level for Global Navigation Satellite System, GNSS, atomic clocks [16]), the temperature difference between these two regions needs to be kept constant to micro-Kelvin levels or better. This temperature-gradient effect is an example of mesoscopic physics, since spatial temperature variations at some level will always exist in vapor-phase systems; and as the example illustrates, exceedingly small fluctuations in temperature gradient can have significant consequences for the 0-0 hyperfine resonance frequencies of atomic clocks.

In the present work we take a closer look at temperature-gradient mesoscopic physics for the ^{87}Rb 0-0 hyperfine transition lineshape. In particular, while the conceptual outline of buffer-gas shifts and broadenings under temperature-gradient conditions is straightforward, the phenomenon has never been explored carefully. Here, our purpose is to investigate the influence of temperature gradients on 0-0 hyperfine transition linewidths and lineshapes under controlled conditions. As will be discussed, we find: (a) that a temperature gradient across a vapor's signal volume has more of an effect on the 0-0 transition linewidth than an equivalent change in the vapor's average temperature, (b) that temperature gradients can produce lineshape asymmetry as well as broadening, (c) that temperature gradients result in a greater sensitivity of the linewidth to power broadening, and (d) that all of these observations can be understood with a relatively simple statistical model of the mesoscopic physics.

In Sec. II, we discuss our experimental arrangement. Then, in Sec. III we present our measurements of the ^{87}Rb 0-0 hyperfine transition lineshape both in the absence and presence of vapor-phase temperature gradients. Finally, in Sec. IV we present results from our model and compare theory with experiment. We anticipate that the results presented here will provide a foundation for the development of next generation vapor-phase atomic clocks, and in particular will provide the basic physics understanding to allow them to finally break into the 10^{-16} frequency stability range [17].

II. EXPERIMENT

Figure 1 is a block diagram of our experimental arrangement. A VCSEL diode laser at $\lambda = 780\,{\rm nm}$ ($\omega_L = 2\pi c/\lambda$) is locked to the $5\,^2S_{1/2}(F_g = 2) \rightarrow 5\,^2P_{3/2}$ transition of ^{87}Rb (i.e., the D_2 transition) in a cell containing isotopically enriched Rb and 10 torr of N_2. In a separate beam, the same laser light is expanded and apertured (to make a reasonably collimated "top-hat" beam) before passing into our resonance cell, which also contains isotopically enriched ^{87}Rb and 10 torr N_2. (Given the relatively large phase noise of VCSEL diode lasers [18], and the not so small diameter of our aperture, we see no evidence of diffraction effects in our experiment or our experimental results.) The beam diameter in the resonance cell is $2R_L \cong 0.27\,{\rm cm}$; the cell has a diameter of $2R_c = 2.5\,{\rm cm}$, and the cell length is $L = 3.8\,{\rm cm}$. This geometry was chosen so that the signal volume diameter would be much smaller than the cell diameter, thereby limiting temperature gradients across the signal volume to the axial direction. The maximum laser power entering the cell is nominally 45 μW.

The cell is located in an oven where we can superimpose a temperature gradient along the cell length, and the oven sits inside a mu-metal tube to limit environmental magnetic fields to the axial direction. (The heating jacket is actually composed of two strip-heaters on each end of the cell.) Magnetic field coils are placed outside the mu-metal tube to impose a controllable, axial quantization axis on the atoms, and these provide a 76 mG magnetic field inside the tube for our experiments. The microwaves are derived from a frequency synthesizer; they pass through a variable attenuator, and then a +30 dB amplifier before passing to a horn that broadcasts the microwave signal to the atoms in the resonance cell. (The maximum forward power at the horn is −11.5 dBm.) In this way, there is no cavity-mode field geometry over the signal volume that could create mesoscopic effects [11]. The transmitted light intensity is detected with a Si photodiode, amplified, and recorded with an averaging oscilloscope.

Figure 2 shows the optical absorption spectrum for the resonance cell at room temperature ($\Theta_c = 24\,^\circ{\rm C}$) taken with extremely low light intensity (i.e., no optical pumping and the laser was unlocked for these measurements): $\eta \equiv [{\rm Rb}]\sigma L = \ln[V_o/V_L]$, where V_o and V_L are the photodiode voltages measured for the light off-resonance [19] and near-resonance, respectively, after passing though the vapor. [Rb] is the rubidium number density, and σ is the (laser-frequency dependent) optical absorption cross-section. The data of Fig. 2 have been calibrated in terms of the cell length and alkali number density at room temperature using the vapor pressure curves of Killian [20] and Ditchburn and Gilmore [21]. These then yield the absorption cross section for the peak of the $F_g = 2$ resonance: $\sigma = (6.6 \pm 2.4) \times 10^{-12}\,{\rm cm}^2$. (By taking the measurement at room temperature, we know the true temperature of the liquid Rb pool in the resonance cell; consequently, the uncertainty is determined solely by the variance in the vapor pressure curves of Killian and Ditchburn and Gilmore.) We note that the two absorption resonances are in the ratio of the ground-state hyperfine level degeneracies (i.e., 3/5) verifying that optical-pumping effects were absent in the absorption spectrum. Additionally, we calibrated the photodiode signal voltage to

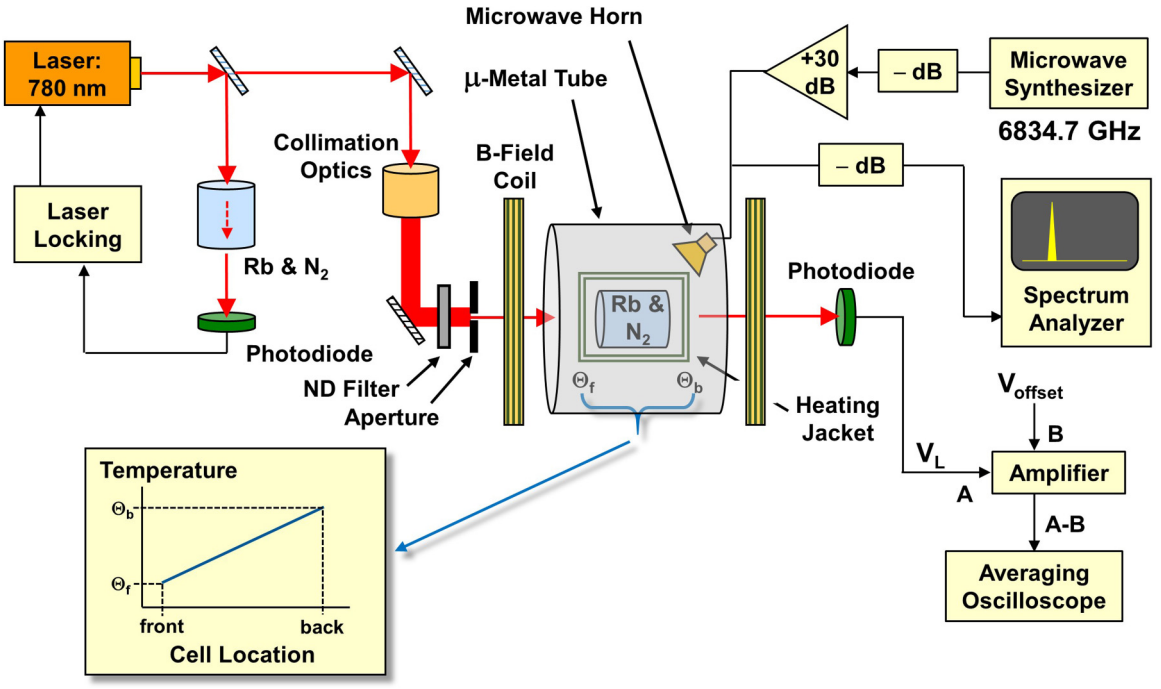

FIG. 1. Experimental arrangement. With heating strips placed on the front and back of the resonance cell (i.e., "heating jacket") we can impose a temperature gradient along the length of the cell. Since the beam diameter is small, the temperature gradient is essentially confined to the axial direction.

laser power within the resonance cell, P_L (accounting for glass transmission losses and with the laser off-resonance): $P_L = \kappa V_o$. Thus, in combination with the optical absorption cross section we had means of defining a photon-absorption rate parameter: $\Gamma_o \equiv \kappa V_L \sigma/(\pi {R_L}^2 \hbar \omega_L)$ [22].

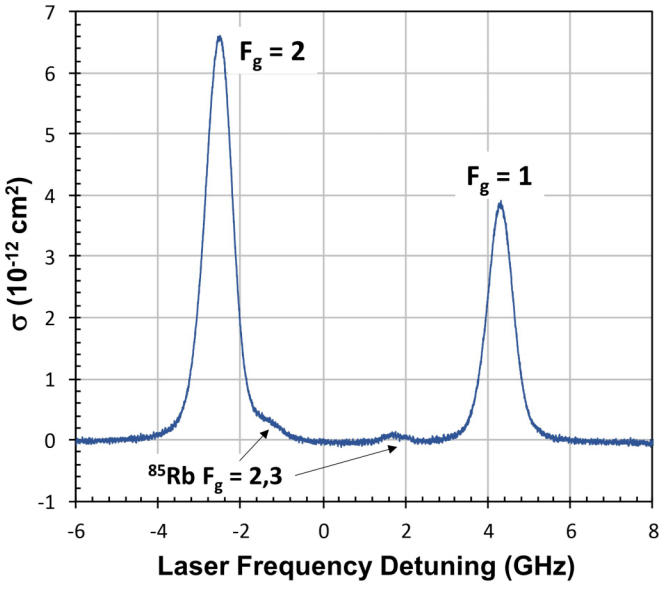

FIG. 2. We measured the laser absorption in the resonance cell as a function of laser frequency by altering the VCSEL injection current. As the measurements were made at room temperature, we had good knowledge of the liquid Rb pool's temperature and hence the Rb vapor density, [Rb]. Dividing the absorption coefficient ($\eta = [\mathrm{Rb}]\sigma L$) by [Rb]$L$ then gave the absorption coefficient, σ.

For each 0-0 hyperfine transition lineshape measurement (with the laser now locked to the D_2 resonance and at higher intensity), we first recorded the amplitude of the 6834.7 MHz microwave signal on the spectrum analyzer shown in Fig. 1, which yielded the microwave power delivered to the horn, $P_{\mu w}$. Additionally, we measured V_L, which yielded Γ_o through the P_L to V_L calibration. We then scanned the microwave frequency ν over the 0-0 hyperfine transition frequency, ν_{hfs}. (The laser was on continuously during these scans.) Finally, taking the natural logarithm of the transmitted light signal yielded the relative change in the $|F_g = 2\rangle$ ^{87}Rb number density as a function of ν, which is our measure of the hyperfine transition lineshape.

Figure 3 shows a typical 0-0 hyperfine transition lineshape for a cell temperature of 44 °C and no temperature gradient. The lineshape is normalized, and we fit that portion of the normalized signal with amplitude greater than 0.5 to a Lorentzian to estimate: (1) the half-width half-maximum (HWHM), $\Delta\nu_{1/2}$, and (2) the frequency for the lineshape's peak, ν_{fit}. Our rationale for focusing on the central portion of the lineshape for our fit, as opposed to the entire lineshape or the lineshape wings, is that the central portion is of critical importance for atomic clocks and other atomic devices [23]. In Fig. 3, the dashed line corresponds to the Lorentzian fit, and it is clear that while the central portion of the 0-0 transition is well described by a Lorentzian, the wings of the actual lineshape fall off slower than a Lorentzian. While we will not discuss the lineshape wings in any great detail, we believe that these are a manifestation of mesoscopic physics: the microscopic quantum dynamics predict a Lorentzian lineshape [24]; we recognize of course that other causes can also lead to non-Lorentzian lineshapes [11,25]. For completeness, we note that for our experiments the average value of $\nu_{\mathrm{fit}} - \nu_o$

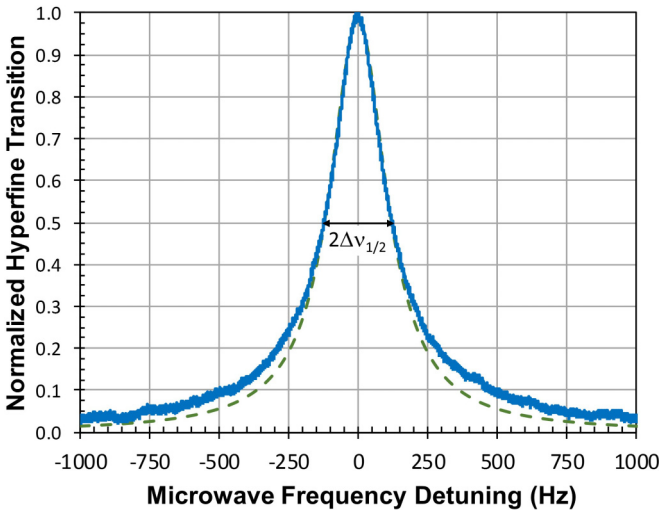

FIG. 3. An example of our measured lineshapes without a temperature gradient. The dashed line is a Lorentzian fit to that portion of the lineshape with amplitude greater than 0.5. For this figure, the abscissa is $\nu - \nu_{\rm fit}$, and we had $\Theta_c = 44\,^{\circ}$C, [Rb]$\sigma L = 1.92$, $P_{\mu w} = 38\,\mu$W, and $\Gamma_o = 7225\,{\rm s}^{-1}$. The half-width half-maximum (HWHM), $\Delta\nu_{1/2}$ was 123 Hz.

(where ν_o is the free atom value of $\nu_{\rm hfs}$) was 5657 Hz, which is indicative of a 10.5 Torr N_2 filled cell [26], consistent with expectations.

In addition to assessing $\Delta\nu_{1/2}$ and $\nu_{\rm fit}$ for our measured lineshapes, we also computed $\nu_{\rm res}$, which is defined as the zero-crossing of the lineshape's derivative (computed numerically). Further, for each experimental run (holding Γ_o constant but varying $P_{\mu w}$), we fit the amplitude of the measured lineshapes to a saturation curve, $(P_{\mu w}/P_{\rm sat})/(1 + P_{\mu w}/P_{\rm sat})$, and in that way estimated the saturation-power for all of our temperature-gradient conditions: no-gradient, positive gradient, and negative gradient (these will be defined more rigorously below). We found no statistically meaningful variation of the saturation power over the three temperature-gradient conditions. Consequently, treating all three temperature-gradient conditions collectively, and recognizing that the saturation power should scale like ${\Gamma_o}^2$, we obtained the relation (with Γ_o in units of ${\rm s}^{-1}$)

$$P_{\rm sat} = (2.9 \pm 1.0) \times 10^{-7}\Gamma_o^2 + (26 \pm 2)\,\mu{\rm W}. \qquad (2)$$

III. RESULTS

A. No temperature gradient

Figure 4(a) shows $\Delta\nu_{1/2}^2$ as a function of microwave power, while Fig. 4(b) shows a lineshape asymmetry parameter, α, as a function of microwave power. The asymmetry parameter is defined by taking the difference between $\nu_{\rm fit}$ and $\nu_{\rm res}$ relative to the lineshape's FWHM:

$$\alpha \equiv \frac{(\nu_{\rm fit} - \nu_{\rm res})}{2\Delta\nu_{1/2}}. \qquad (3)$$

Consequently, α is a fractional measure of the lineshape's skewness with positive values indicating that the lineshape has

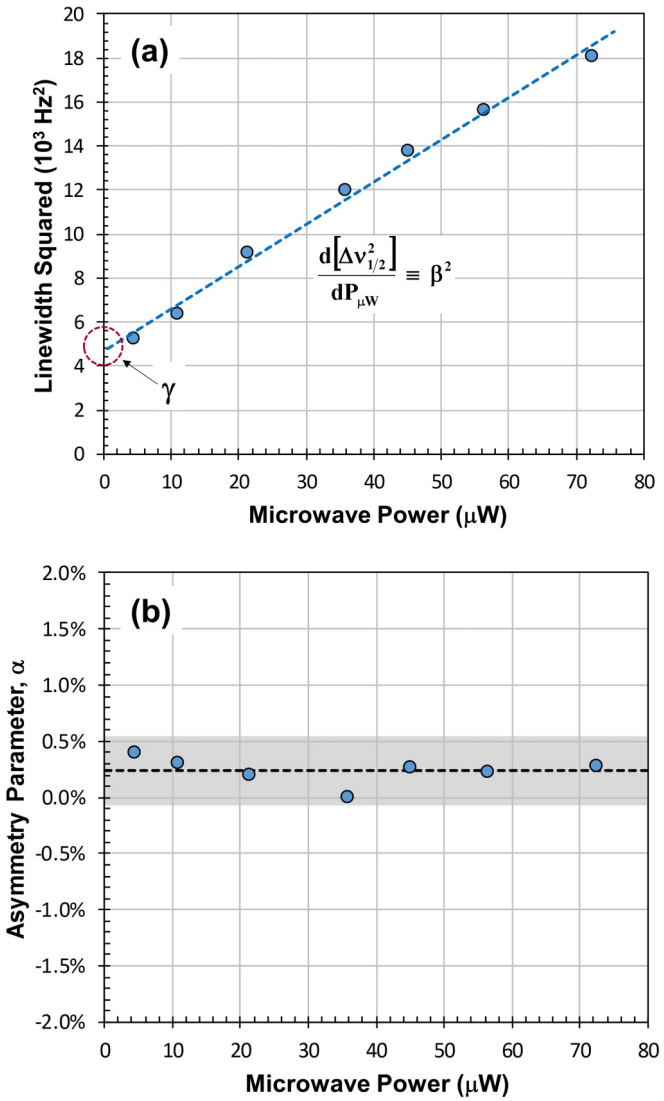

FIG. 4. (a) For the case of $\Theta_c = 44\,^{\circ}$C, no temperature gradient, [Rb]$\sigma L = 1.92$, and $\Gamma_o = 699\,{\rm s}^{-1}$, this figure shows the linewidth squared as a function of microwave power. The intercept corresponds to the residual HWHM, γ, which is affected by collisional processes and light-broadening (due to optical pumping); the slope yields β^2. (b) The asymmetry parameter α as a function of microwave power. The asymmetry parameter is independent of microwave power, and for this experiment indistinguishable from zero at the 95% confidence level. (The gray region corresponds to the 95% confidence interval and the average is indicated by the dashed line.)

an asymmetry (i.e., a larger wing) on the high-frequency side of the resonance.

From the intercept of the straight line relationship between $\Delta\nu_{1/2}^2$ and $P_{\mu w}$ shown in Fig. 4(a), we estimated the transition's microwave-independent linewidth, γ, which is a measure of collisional, diffusion, and light-broadening processes [27]. The slope of the line is a power-broadening "linewidth enhancement factor," which we label as β^2. For a two-level atom, $\beta = (T_1/T_2)^{1/2}$, where T_2 and T_1 are the transverse (i.e., dephasing) and longitudinal relaxation times for the system, respectively [28], while for multilevel systems β can have a more complicated relationship with these relaxation times

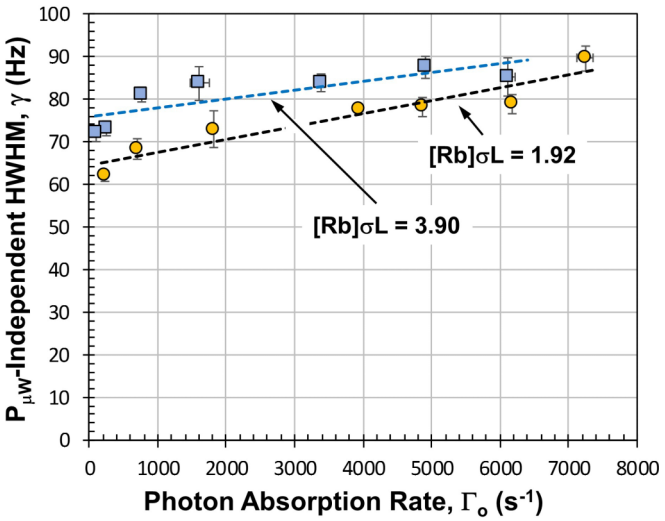

FIG. 5. Microwave power independent linewidth, γ, as a function of the optical photon absorption rate, Γ_o: squares correspond to $\Theta_c = 54\,^{\circ}\mathrm{C}$, while circles correspond to $\Theta_c = 44\,^{\circ}\mathrm{C}$. While the slopes are not distinguishable at the 95% confidence level, the difference in the intercepts is significant, and traces back to a difference in spin-exchange dephasing of the 0-0 hyperfine transition.

[25]. For the parameters of Fig. 4(a) we have $\gamma = (68.3 \pm 2.4)\,\mathrm{Hz}$, and $\beta = (13.9 \pm 0.3)\,\mathrm{Hz}/\mu\mathrm{W}^{1/2}$. Additionally, from Fig. 4(b) we see that α is very small: $\alpha = (0.23 \pm 0.12)\%$. Thus, in the absence of a temperature gradient we have the comforting result that the lineshape shows little to no asymmetry. Moreover, as the slope of the α versus $P_{\mu w}$ line is indistinguishable from zero at the 95% confidence level (i.e., $\partial\alpha/\partial P_{\mu w} = -(1.2 \pm 2.2) \times 10^{-3}\%/\mu\mathrm{W}$), we have evidence that the symmetry of the lineshape is independent of microwave power.

Figure 5 shows γ as a function of photon absorption rate for two different temperatures: $\Theta_c = 44\,^{\circ}\mathrm{C}$ with a measured $[\mathrm{Rb}]\sigma L = 1.92 \pm 0.17$, and $\Theta_c = 54\,^{\circ}\mathrm{C}$ with a measured $[\mathrm{Rb}]\sigma L = 3.90 \pm 0.29$. The slopes are indistinguishable at the 95% confidence level and are likely strongly influenced by diffusional modes in the resonance cell (a separate mesoscopic effect) [17,29]. Alternatively, the intercepts are clearly different.

Defining γ_o as the light-independent and microwave-power independent linewidth we have

$$\gamma_o \equiv \begin{cases} (64.6 \pm 2.1)\mathrm{Hz} & [\mathrm{Rb}]\sigma L = 1.92 \\ (75.9 \pm 2.2)\mathrm{Hz} & [\mathrm{Rb}]\sigma L = 3.90 \end{cases}. \tag{4}$$

This difference can be explained as a consequence of Rb-Rb spin-exchange. To proceed, we write γ_o as $\gamma_o' + \gamma_{\mathrm{ex}} = \gamma_o' + (\frac{6I+1}{8I+4})[\mathrm{Rb}]\sigma_{\mathrm{ex}}\bar{v}$ [30], where γ_o' is the dephasing rate for all processes other than spin-exchange, σ_{ex} is the spin-exchange cross section for Rb with $\bar{v}$ the mean relative speed between two Rb atoms, and I the nuclear spin. Assuming γ_o' is independent of Θ_c, the difference between the two values of γ_o is then given by

$$\gamma_o(54\,^{\circ}\mathrm{C}) - \gamma_o(44\,^{\circ}\mathrm{C}) = \left(\frac{6I+1}{8I+4}\right)\sigma_{\mathrm{ex}}\bar{v}\{[\mathrm{Rb}]_{54\,^{\circ}\mathrm{C}} - [\mathrm{Rb}]_{44\,^{\circ}\mathrm{C}}\}, \tag{5}$$

from which we can determine the spin-exchange cross-section: $\sigma_{\mathrm{ex}} = (1.5 \pm 0.4) \times 10^{-14}\,\mathrm{cm}^2$. This result compares well with the theoretical value of $1.6 \times 10^{-14}\,\mathrm{cm}^2$ [31], indicating that in the absence of a temperature gradient the primary temperature-dependent effect appearing in the linewidth arises from spin-exchange, which for a doubling of $[\mathrm{Rb}]\sigma L$ only adds about 10 Hz to γ_o.

B. Temperature gradients

To accentuate the influence of a temperature gradient on 0-0 hyperfine transition lineshapes, we imposed an approximately 10 °C temperature gradient across the cell. Seven thermistors were placed on the cell: one at $z/L \equiv \zeta = 0$ (i.e., the front of the cell at the laser beam entrance), one at $\zeta = 1$, and five around the cell center at $\zeta = 0.5$. Primarily, the thermistors near the cell center were meant to give us some assessment of possible radial temperature gradients, which we estimated as roughly 0.3 °C over the signal volume for this magnitude axial temperature gradient. Unfortunately, the five centrally located thermistors could not give us a useful estimate of the actual vapor temperature on axis at $\zeta = 0.5$, since the temperature measurements (located on the cell's outside glass wall) were relatively far removed from the location of the signal volume.

Though we only had two reliable measurements of the temperature gradient along the signal volume (i.e., $\zeta = 0$ and $\zeta = 1$) [32], we nevertheless allowed for the possibility that the temperature gradient might be nonlinear:

$$\Theta_z = \Theta_0 + A\zeta(1 + f\zeta). \tag{6a}$$

Here, f is uniquely determined by Θ_L, Θ_0, and A:

$$f = \frac{\Theta_L - \Theta_0}{A} - 1. \tag{6b}$$

In our analyses, we treat A as a parameter to be determined by experiment. Nevertheless, given our experimental arrangement we expected Θ_z to be close to linear in ζ over the cell length, which implied that we should expect the A values to result in $f < 1$.

Assuming an ideal buffer gas, this temperature gradient profile implies a buffer-gas density gradient (and thereby a collision-shift gradient) of

$$\frac{[\mathrm{BG}]_z - [\mathrm{BG}]_0}{[\mathrm{BG}]_0} = \frac{\Theta_0}{\Theta_z} - 1 = -\frac{A\zeta(1 + f\zeta)}{\Theta_0 + A\zeta(1 + f\zeta)} \tag{7}$$

(where Θ is in Kelvin for this equation). Note that for $|\Theta_L - \Theta_0| = 10\,^{\circ}\mathrm{C}$, the relative size of the buffer-gas density change is roughly 3% over the signal volume. Though this may seem quite small, it should be taken in the context of the total buffer-gas collision shift relative to the linewidth of the 0-0 hyperfine transition. In the present case, the total buffer-gas collision shift is about 5660 Hz, so that 3% of this shift is about 170 Hz, and such a shift is quite large when compared to the 65 Hz linewidth of the 0-0 transition in the absence of a temperature gradient.

For a fair comparison with the no-gradient results, we carefully set temperatures across the signal volume so that the average value of $[\mathrm{Rb}]\sigma L$ was as close as possible to the

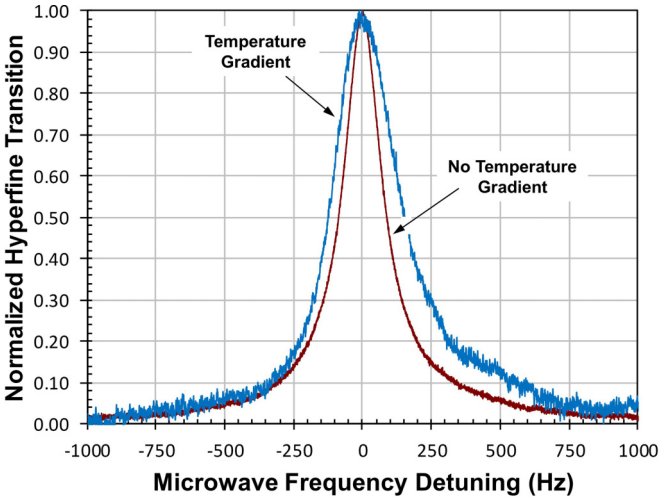

FIG. 6. Comparison of the 0-0 hyperfine transition lineshapes under nearly similar conditions with and without an 11 °C positive temperature variation across the length of the resonance cell (i.e., $\Theta_L > \Theta_0$). For the case of no temperature gradient, $[\mathrm{Rb}]\sigma L = 1.92$, $\Gamma_o = 1830\,\mathrm{s}^{-1}$, and $P_{\mu w} = 13\,\mu\mathrm{W}$; for the case with a temperature gradient, $\langle[\mathrm{Rb}]\sigma L\rangle = 1.92$, $\Gamma_o = 1110\,\mathrm{s}^{-1}$, and $P_{\mu w} = 17\,\mu\mathrm{W}$.

no-gradient conditions:

$$\ln\left[\frac{V_o}{V_L}\right] = \sigma\int_0^L [\mathrm{Rb}]_z dz \equiv \langle[\mathrm{Rb}]\rangle\sigma L. \tag{8}$$

For our negative gradient experiments, we had $\Theta_0 = 50.2\,^\circ\mathrm{C}$, $\Theta_L = 38.3\,^\circ\mathrm{C}$, and $\langle[\mathrm{Rb}]\rangle\sigma L = 1.90 \pm 0.15$; for our positive gradient experiments we had $\Theta_0 = 40.8\,^\circ\mathrm{C}$, $\Theta_L = 51.6\,^\circ\mathrm{C}$, and $\langle[\mathrm{Rb}]\rangle\sigma L = 1.92 \pm 0.17$. Thus, the average contributions of spin-exchange to the lineshape should differ very little among no-gradient, positive-gradient, and negative-gradient temperature conditions.

Figures 6 and 7 are comparisons of the 0-0 hyperfine transition lineshape under nearly identical conditions *with* and *without* a positive temperature gradient across the length of the signal volume (i.e., $\Theta_L - \Theta_0 = 11\,^\circ\mathrm{C}$). Examining Fig. 6 it is clear that temperature gradients give rise to a broadening of the resonance lineshape and an asymmetry. Similar asymmetric lineshapes were observed with negative temperature gradients, and for both positive and negative gradients the asymmetric wing extended to positive microwave-frequency detunings. From Fig. 7 we see that: (1) even in the presence of a temperature gradient the square of the linewidth appears to have a linear dependence on $P_{\mu w}$, (2) the increased broadening extends to zero microwave power (i.e., the Rabi frequency, Ω, equals zero), and (3) a temperature gradient results in a larger value of the linewidth-enhancement factor, β.

As suggested by the data of Fig. 6, the data presented in Fig. 8 show that regardless of photon absorption rate, Γ_o, linewidths are broadened by the presence of a temperature gradient. Figures 9(a) and 9(b) compare the light-independent linewidths, γ_o, and the slopes (*i.e.*, $d\gamma/d\Gamma_o$), respectively, for the three temperature-gradient conditions. Error bars indicate 95% confidence intervals. There appears to be a clear increase in γ_o due to the presence of a temperature gradient, which in the present case is by a factor of 1.6. However, at the 95% confidence level there appears to be no difference in the increased linewidths for positive versus negative temperature gradient conditions. Regarding the estimated values of $d\gamma/d\Gamma_o$, there is no evidence of a difference among the

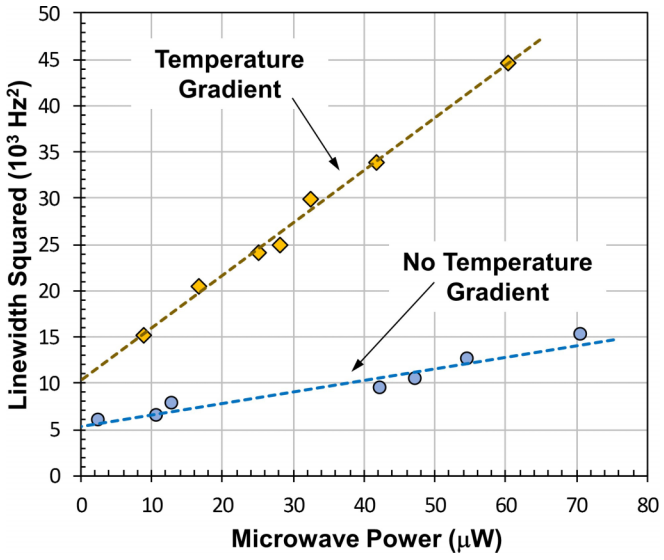

FIG. 7. Comparison of the microwave power dependence of the 0-0 hyperfine transition lineshape under nearly similar conditions with and without an 11 °C positive temperature variation across the length of the resonance cell (i.e., $\Theta_L > \Theta_0$). For the case of no temperature gradient, $[\mathrm{Rb}]\sigma L = 1.92$ and $\Gamma_o = 1830\,\mathrm{s}^{-1}$; for the case with a temperature gradient, $\langle[\mathrm{Rb}]\sigma L\rangle = 1.92$ and $\Gamma_o = 1110\,\mathrm{s}^{-1}$. The slope of the least-squares fits yields β.

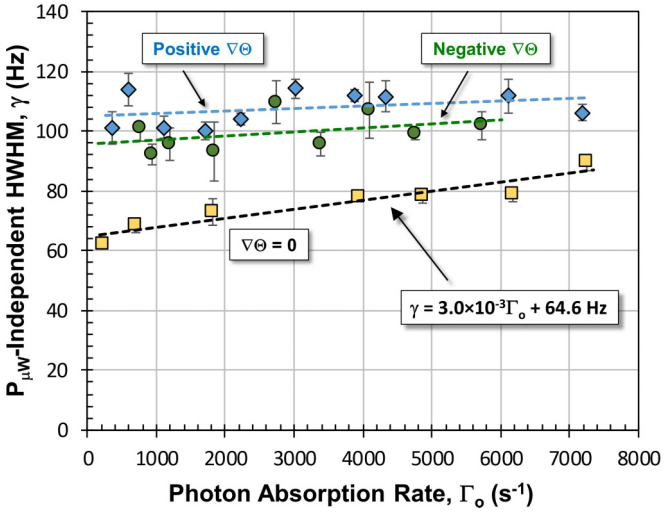

FIG. 8. Residual linewidth, γ (i.e., $P_{\mu w} \to 0$) as a function of photon absorption rate, Γ_o: squares $\Rightarrow$ no temperature gradient, diamonds $\Rightarrow$ negative temperature gradient, and circles $\Rightarrow$ positive temperature gradient. Temperature gradients clearly increase the linewidth of the 0-0 transition, and when compared with Fig. 5 the effect of temperature gradients seems to be larger than a simple increase of the mean vapor temperature. Also shown is the equation for the least squares fit of γ to Γ_o under no-gradient conditions: $\gamma = 3.0 \times 10^{-3}\Gamma_o + 64.6\,\mathrm{Hz}$.

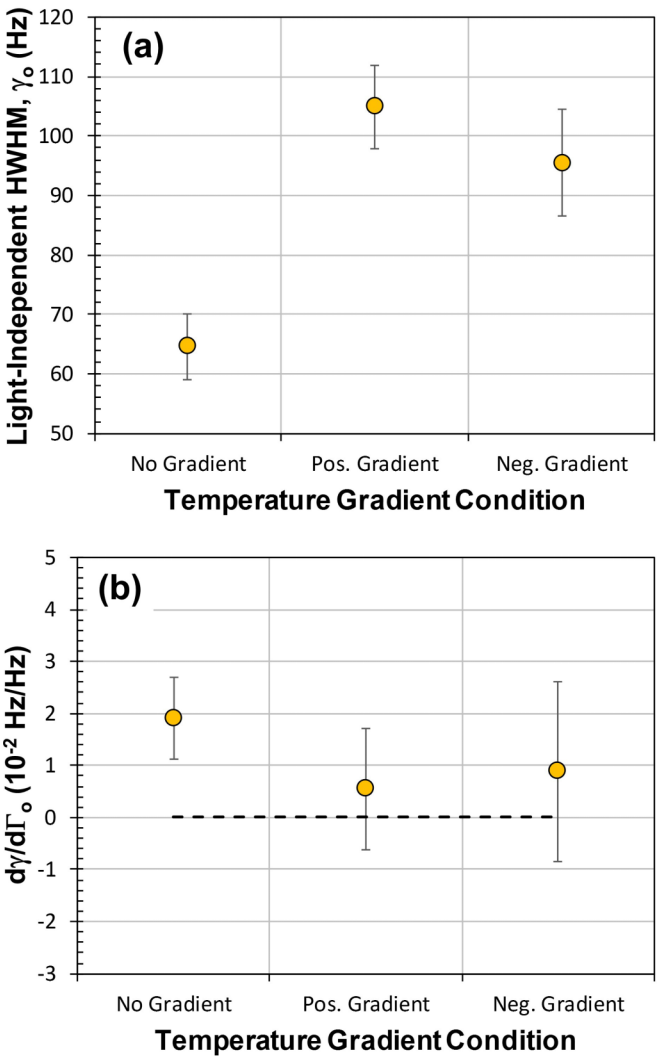

FIG. 9. (a) Light-independent HWHM, γ_o, as a function of temperature gradient condition; error bars correspond to 95% confidence intervals. (b) In units of Hz/Hz this figure shows $d\gamma/d\Gamma_o$ as a function of temperature gradient condition; again, error bars correspond to 95% confidence intervals.

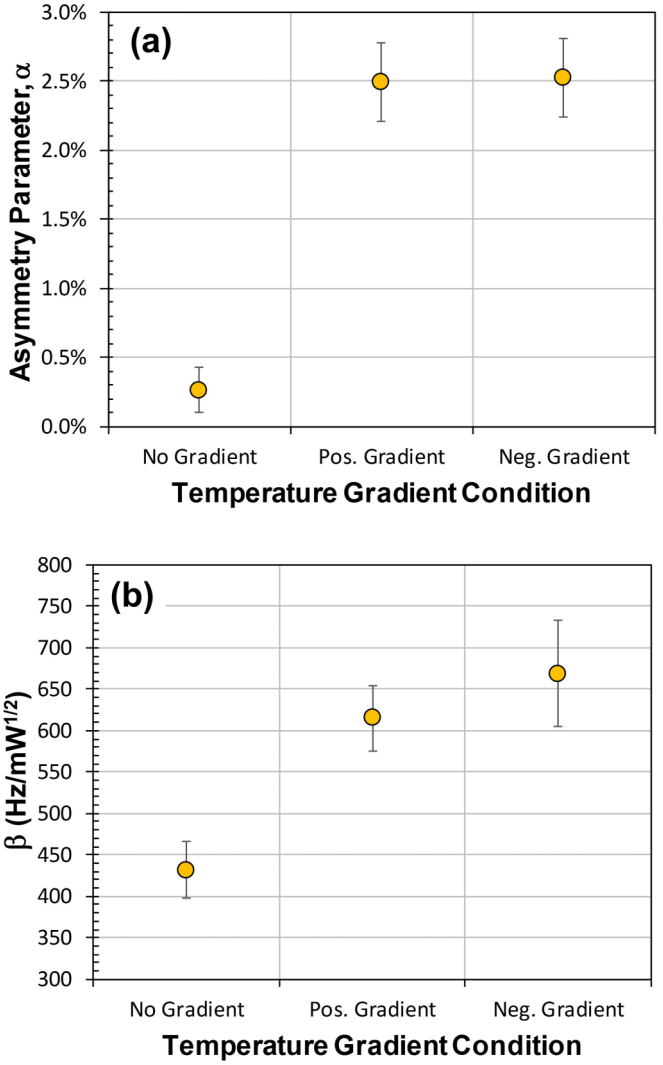

FIG. 10. (a) Asymmetry parameter, α, averaged over photon absorption rate, Γ_o, and microwave power, $P_{\mu w}$, as a function of temperature-gradient condition. There is clearly a gradient-induced lineshape asymmetry, and we suspect that the slight asymmetry under "no gradient" conditions is a manifestation of our inability to completely eliminate temperature gradients in the experiment. (b) The microwave-power dependence of the linewidth enhancement factor β as a function of temperature-gradient condition. There is a clear effect of the temperature gradient on β, though we find no (statistically significant) difference in β for positive and negative gradient conditions. Error bars correspond to 95% confidence intervals.

three temperature-gradient conditions at the 95% confidence level.

Figures 10(a) and 10(b) show the asymmetry parameter α and the linewidth-enhancement factor β for the three temperature-gradient conditions, respectively, averaged over photon absorption rate, Γ_o (and microwave power in the case of α). The data showed no significant influence of Γ_o on either α or β under any of the temperature-gradient conditions, and there was no statistically significant effect of $P_{\mu w}$ on α. As Fig. 10 shows, temperature gradients create lineshape asymmetry and lead to enhanced microwave power broadening. While there is a very slight residual asymmetry under our no-gradient conditions, we assume that this is due to a slight temperature gradient that we were unable to completely eliminate. Clearly, however, the asymmetry under explicit positive and negative temperature-gradient conditions is considerably larger. For both α and β, we see no difference in these parameters for positive versus negative temperature-gradient conditions.

IV. STATISTICAL THEORY

To describe the effects of mesoscopic physics on the 0-0 hyperfine transition lineshape, one could obviously set up the complete spatiotemporal density matrix equations for the problem, accounting for diffusional relaxation of hyperfine polarization, optical pumping, collisional dephasing/shifts, etc., and then give those rates (where necessary) a functional dependence on spatial position. Through that effort, one could

certainly compare detailed theory with experiment. However, given the complexity of the (likely nonlinear) density matrix equations, and the necessity of solving those equations numerically, it is not at all clear that such a procedure would provide any great intuitive understanding of the problem. Here, our focus is on insight, and to that end we will find a statistical approach advantageous. Our goal is threefold: to develop some intuition regarding the underlying physics giving rise to temperature-gradient induced increases in (a) line broadening and (b) β values and (c) to understand the origin of lineshape asymmetry.

A. Overview

To proceed, we follow the normal derivation of Beer's law, and consider the relative change in light intensity at axial location ζ, $\delta I_\zeta / I_\zeta$, caused by photon absorption from a thin axial slice of vapor, δz. We write the number-density of atoms in the optically absorbing state as $\eta(\nu - \nu_\zeta)$[Rb], where $\eta(\nu - \nu_\zeta)$ is the fraction of atoms in the absorbing state as a function of microwave detuning from the 0-0 hyperfine resonant frequency at axial location ζ (indicated as ν_ζ) obtaining

$$\delta I_\zeta = -I_\zeta \eta(\nu - \nu_\zeta)[\mathrm{Rb}]\sigma \delta z. \tag{9}$$

Integrating Eq. (9) across the vapor length, we then obtain

$$I(L, \nu) = I_0 e^{-[\mathrm{Rb}]\sigma L \int_0^1 \eta(\nu,\zeta)\mathrm{d}\zeta} = I_0 e^{-[\mathrm{Rb}]\sigma L \langle \eta(\nu)\rangle}, \tag{10}$$

The important point to note from Eq. (10) is that the light intensity transmitted by the vapor (our observable for the 0-0 hyperfine resonance) corresponds to a statistical quantity: the value of $\eta(\nu,\zeta)$ averaged over the signal volume.

As a result of this recognition, we can make a conceptual switch. Rather than considering the light-beam's propagation through a vapor of spatially varying $\eta(\nu)$ values, we consider a statistical ensemble of independent and differing $\eta(\nu)$ values, and average over the ensemble. Within the ensemble, we label each of the $\eta(\nu)$ values by $\zeta : \eta(\nu) \to \eta_\zeta(\nu)$, where ζ is now a parameter that distinguishes distinct realizations of $\eta(\nu)$.

In the average of Eq. (10), different regions of the vapor will have a greater or lesser effect on the transmitted light depending on the degree of optical pumping in that region (i.e., the light intensity in that region) and the manner in which diffusion limits the efficacy of optical pumping in that region. To capture this variability in the statistical approach, we allow the number of realizations in the ensemble defined by a specific value of ζ, M_ζ, to vary. Thus, to determine $\langle \eta(\nu)\rangle$ we perform a weighted average over the ensemble:

$$\langle \eta(\nu)\rangle = \sum_\zeta W_\zeta \eta_\zeta(\nu) \to \int W_\zeta \eta_\zeta(\nu) d\zeta, \tag{11}$$

with the weighting factor, W_ζ, given by $M_\zeta / \int M_\zeta d\zeta$.

If there were no variation of η with axial position, then all the $\eta_\zeta(\nu)$ in the ensemble would be equivalent, and we could write for all ζ

$$\eta_\zeta(\nu) = \Lambda + BL(\nu - \nu_{\mathrm{hfs}}), \tag{12}$$

where Λ captures the effect of optical pumping alone on the number-density of atoms in the optically absorbing state (with $0 \leqslant \Lambda \leqslant 1$); B captures the influence of the 0-0 magnetic-resonance on the return of optically pumped atoms to the absorbing state (with $0 \leqslant B \leqslant 1 - \Lambda$), and $L(\nu - \nu_{\mathrm{hfs}})$ is a normalized-amplitude Lorentzian centered on the hyperfine resonance frequency. In the case that η *does* depend on axial position, we should therefore write

$$\eta_\zeta(\nu) = \Lambda_\zeta + B_\zeta L(\nu - \nu_\zeta), \tag{13a}$$

$$\langle \eta(\nu)\rangle = \int_0^1 [\Lambda_\zeta + B_\zeta L(\nu - \nu_\zeta)] d\zeta = \langle \Lambda \rangle + \int_0^1 B_\zeta L(\nu - \nu_\zeta) d\zeta. \tag{13b}$$

Notice, that the second term on the right-hand-side of Eq. (13b) has the appearance of a weighted average similar to Eq. (11): $W_\zeta \to B_\zeta$.

In the statistical approach, the crux of the theoretical problem is determining the appropriate form and values of B_ζ, along with the form of $L(\nu - \nu_\zeta)$, and this of course is a nontrivial problem. However, it is nonetheless possible to make a first-order educated guess as to B_ζ and $L(\nu - \nu_\zeta)$, and to the extent that those educated guesses lead to results in reasonable agreement with experiment insight into the underlying mesoscopic physics will have been gained. To that end, we expect B_ζ to depend on the degree of optical pumping at ζ, and the manner in which axial diffusion places boundary-value limits on optical pumping's efficacy. Thus, we will take $B_\zeta \cong B_o W_{\mathrm{op}}(\zeta) W_{\mathrm{dif}}(\zeta)$, where W_{op} and W_{dif} are independent optical-pumping and diffusional weighting functions, respectively.

For the optical-pumping weight function we consider simple saturation of the optical-pumping process:

$$W_{\mathrm{op}}(\zeta) = \frac{T_1 \Gamma_o(\zeta)}{1 + T_1 \Gamma_o(\zeta)} \cong \frac{T_1 \Gamma_o e^{-[\mathrm{Rb}]\sigma L \zeta}}{1 + T_1 \Gamma_o e^{-[\mathrm{Rb}]\sigma L \zeta}}, \tag{14}$$

where we have implicitly assumed that to first-order the effects of optical pumping on the absorbing-state number density can be ignored (i.e., $\langle \Lambda \rangle \cong 1$). Also, we define T_1 as the longitudinal relaxation time of the 0-0 transition, which is assumed independent of ζ. Strictly speaking, T_1 will depend on the rate of buffer-gas collisions (BG) and Rb-Rb spin-exchange collisions (SE): $T_1^{-1} = T_1^{-1}(BG) + T_1^{-1}(SE)$. Ignoring for the moment Rb-Rb spin-exchange, since it only contributes about 10 Hz to T_1^{-1}, we note that as the buffer-gas density varies axially so too will T_1(BG). However, whereas a 3% change in the buffer-gas collision shift is significant when compared to the narrow linewidth of the 0-0 resonance, a 3% change in its relaxation rate is not. Taking $\gamma_o = T_1^{-1}(BG) + (\frac{6I+1}{8I+4})[\mathrm{Rb}]\sigma_{\mathrm{ex}} \bar{v}$ in the no-gradient situation, we obtain $T_1(\mathrm{BG}) \cong 2.6\,\mathrm{ms}$ for our $[\mathrm{Rb}]\sigma L = 1.92$ conditions, and this only varies by 3% over the signal volume. (Similar arguments hold for spin-exchange.)

To obtain an intuitive expression for the axial-diffusion weight function, $W_{\mathrm{dif}}(\zeta)$, we raise the first-order axial

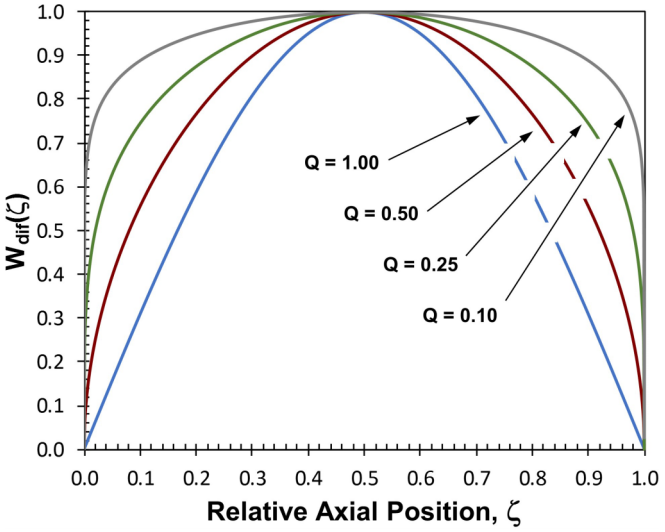

FIG. 11. Various profiles of the axial diffusion weighting function, $W_{\rm dif}(\zeta) = \sin^{Q}(\pi\zeta)$ for differing values of Q.

diffusion mode to the Qth power:

$$W_{\rm dif}(\zeta) = \sin^{Q}(\pi\zeta), \tag{15}$$

with $0 < Q \leqslant 1$. $W_{\rm dif}(\zeta)$ is illustrated in Fig. 11 for several values of Q, where it can be seen that small values of Q indicate a nonnegligible role for high-order axial modes in the diffusion process [33].

Finally, though we could appeal to the Generalized-Vanier theory [25] to write an expression for $L(\nu - \nu_\zeta)$, it will be more illuminating for present purposes to reduce the problem to that of a two-level atom. We therefore write

$$L(\nu - \nu_\zeta) = \frac{\gamma_2^2 + \left({}^{T_1}/_{T_2^*}\right)\Omega^2}{\gamma_2^2 + \left({}^{T_1}/_{T_2^*}\right)\Omega^2 + (\nu - \nu_\zeta)^2}. \tag{16}$$

In this expression, γ_2 is the dephasing rate in the absence of a temperature gradient, while T_2^* is a transverse relaxation time in the presence of inhomogeneous broadening (arising from the spatially varying collision shift). Both γ_2 and T_2^* are considered independent of ζ for the same reasons as T_1. Notice that in this expression we have distinguished $1/T_2^*$ from γ_2, as $1/T_2^*$ takes account of the temperature gradient's influence on power broadening *through* dephasing. (This will be clarified below.)

The observed lineshape, $L_{\rm obs}(\nu)$, is obtained from $\ln[I(L,\nu)/I_0]$ via Eqs. (10) and (13b), so that

$$L_{\rm obs}(\nu) \equiv \int_0^1 W_{\rm op}(\zeta) W_{\rm dif}(\zeta) L(\nu - \nu_\zeta) d\zeta. \tag{17}$$

In the limit $\Omega/\gamma_2 \ll 1$ and $\Gamma_o T_1 \ll 1$ (i.e., small microwave power and light intensity), the observed lineshape reduces to

$$\lim_{\substack{\Omega\to 0\\ \Gamma_o\to 0}} L_{\rm obs}(\nu) = T_1\Gamma_o\gamma_2^2 \int_0^1 \left\{ \frac{e^{-[{\rm Rb}]\sigma L\zeta}\sin^{Q}(\pi\zeta)d\zeta}{\gamma_2^2 + (\nu - \nu_0(\Theta_0/\Theta_\zeta))^2} \right\}, \tag{18}$$

where ν_0 refers to the collision shift at $\zeta = 0$ and Θ values are in Kelvin. Notice that in the absence of a temperature gradient (i.e., $\Theta_\zeta \to \Theta_0$ for all ζ), Eq. (18) reduces to a simple Lorentzian lineshape of halfwidth γ_2.

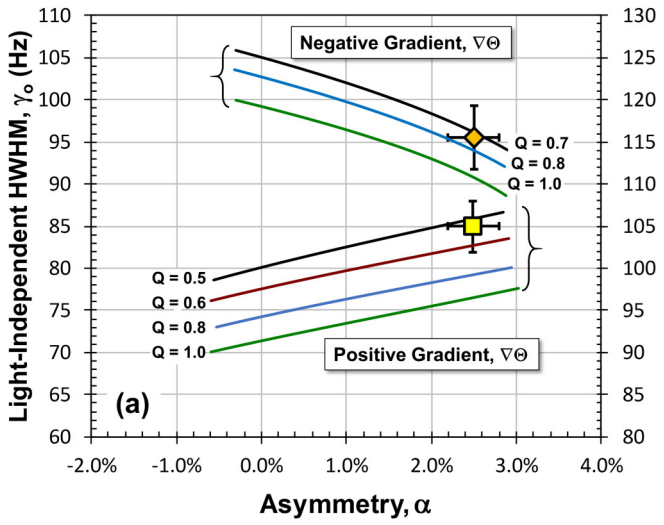

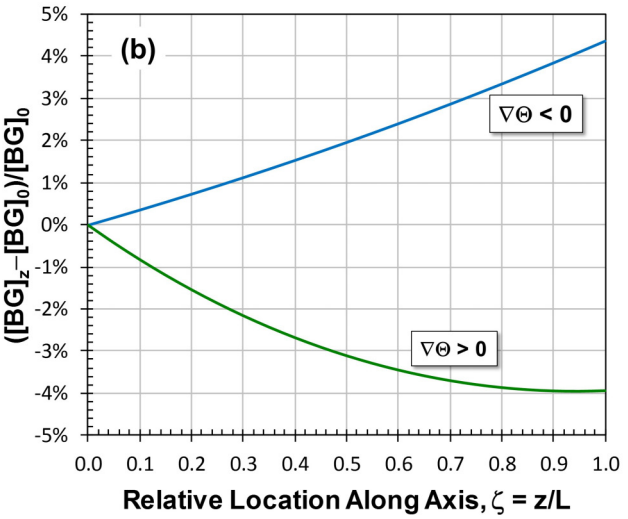

FIG. 12. (a) Diamond $\Rightarrow (\gamma_o, \alpha)$ value for the experimental negative gradient; square $\Rightarrow (\gamma_o, \alpha)$ value for the experimental positive gradient. The various curves are theoretical pairs (γ_o,α) varying Q and A as free parameters. The closest theoretical fit to the data provides an estimate of Q and A: for $\nabla\Theta < 0$ we have $Q = 0.7$ and $A = -10$, while for $\nabla\Theta > 0$ we have $Q = 0.5$ and $A = 23$. (b) Taking the A and Q values determined from (a), we plot the estimates of the buffer-gas density gradient in the resonance cell.

B. Computational results: $\Omega < \gamma_2$

To make quantitative predictions with the statistical theory, we require estimates of Q and A for use in Eqs. (6) and (15). To this end, Fig. 12(a) provides theoretical plots of γ_o versus α for positive and negative gradients (taking Θ_L and Θ_0 from the measured values) along with two data points based on our measurements (i.e., $P_{\mu w}$ and $\Gamma_o \to 0$). For the theoretical curves, we first chose values for Q and A. Then, considering the Ω, $\Gamma_o \to 0$ limit of the statistical theory we computed the lineshape from Eq. (18), and similar to our experimental procedure determined γ_o and α from the computed lineshape.

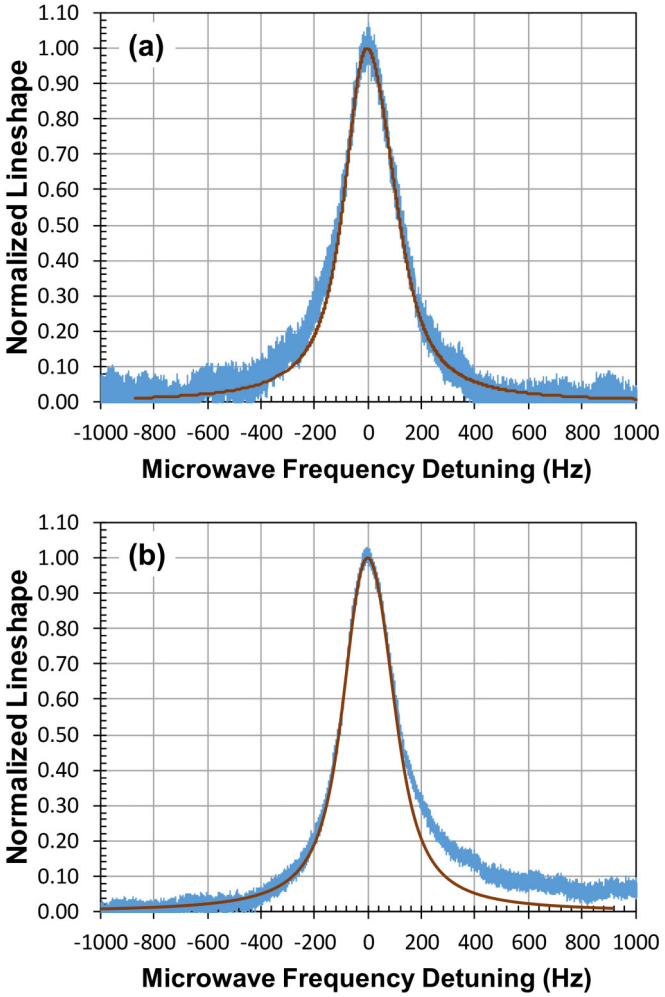

FIG. 13. (a) Comparison of theoretical and experimental lineshapes for low microwave power, but high light intensity under negative temperature gradient conditions ($\Gamma_o = 5720\,\mathrm{s}^{-1}$); (b) same as (a) except for positive temperature gradient conditions ($\Gamma_o = 7180\,\mathrm{s}^{-1}$).

The theoretical predictions closest to experiment provide our estimates of Q and A: for $\nabla\Theta < 0$ we obtain $Q = 0.7$, $A = -10$, and $f = 0.19$; while for $\nabla\Theta > 0$ we obtain $Q = 0.5$, $A = 23$, and $f = -0.53$. As anticipated, the results are consistent with a nearly linear temperature gradient (i.e., $f < 1$), which provides some confidence that our estimates of Q and A are reasonable. The resulting density gradients for these temperature profiles are plotted in Fig. 12(b).

For comparison purposes, Fig. 13 shows experimental and theoretical lineshapes for low microwave power but high light intensity in the case of both a negative ($\Gamma_o = 5720\,\mathrm{s}^{-1}$) and a positive ($\Gamma_o = 7180\,\mathrm{s}^{-1}$) temperature gradient. In both cases the agreement is respectable, though better in the wings of the line for a negative temperature gradient. Figure 14 shows the predicted values of γ and α for the positive and negative temperature gradient conditions along with the experimental results. For the computations, γ_2 in Eq. (15) was taken as a linear function of the light intensity, with a slope and intercept derived from the $\nabla\Theta = 0$ conditions (see Fig. 8). (This procedure was also employed to generate the theoretical

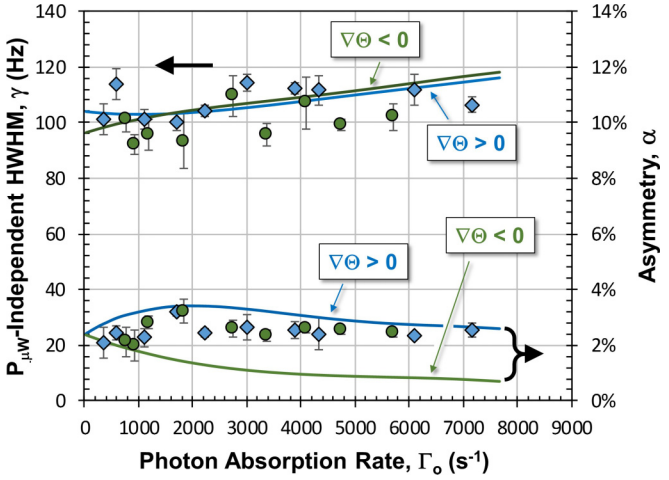

FIG. 14. Comparison between theory and experiment for the 0-0 hyperfine transition linewidth γ, and asymmetry α: diamonds $\Rightarrow$ positive temperature gradient, circles $\Rightarrow$ negative temperature gradient.

lineshapes of Fig. 13.) The predicted linewidth values under temperature gradient conditions agree reasonably well with experiment. Interestingly, theory predicts a slight nonlinear dependence of γ on Γ_o for low light-intensity levels. With regard to the asymmetry parameter α, theory and experiment are a bit more disparate, but nevertheless in reasonable agreement given our fairly simplistic descriptions of the weighting functions $W_{\mathrm{op}}(\zeta)$ and $W_{\mathrm{diff}}(\zeta)$.

C. Computational results: $\Omega > \gamma_2$

Before applying our theory to strong-field conditions, there are two points that need to be clarified. The first relates to the physical interpretation of the linewidth-enhancement factor in the case of homogeneous broadening, T_1/T_2. Clearly, in the presence of a perturbing microwave field that couples two quantum states (in our case $|F = a = I + 1/2,\ m_{\mathrm{F}} = 0\rangle$ and $|F = b = I - 1/2,\ m_{\mathrm{F}} = 0\rangle$) a superposition state is created: $|\Phi\rangle = [|a, 0\rangle + |b, 0\rangle]/2^{1/2}$. This superposition state lasts for a mean time T_1, because every longitudinal relaxation event collapses the superposition-state wavefunction to one of the unperturbed hyperfine eigenstates. $1/T_2$ is the dephasing rate of atomic coherence or stating that differently the rate at which the phase of different superposition states "slip" relative to one another. Thus, T_1/T_2 is the total average phase-slip of a superposition-state wavefunction over the course of its lifetime.

The second point relates to our development of the statistical theory from Eqs. (9) and (10), and the recognition that the observed 0-0 lineshape derives from a light beam's attenuation by sequential layers of the absorbing medium. It was essentially sequential absorption (i.e., the integral over $\eta(\nu,\zeta)$ in Eq. (1)) that allowed us to treat different spatial regions within the vapor as separate and distinct. However, under microwave-saturation conditions one cannot ignore the overall coherence of the many superposition states created by the field, which has the effect of mixing those distinct spatial regions in the transmitted light.

To illustrate the point, consider a transient nutation double-resonance experiment: turn on a strong microwave field instantaneously and observe the transmitted light as a function of time. The optical absorption, $\eta(t)$, will display damped oscillations sitting on an exponentially rising background: $\eta(t) \sim \eta_\infty - \delta_\eta e^{-t/\tau_b}\sin(\omega_R t + \phi)$, where ω_R will be some average of the Rabi nutation frequencies over the entire sample: $[\Omega^2 + (\nu - \nu_\zeta)^2]^{1/2}$. The decay time, τ_b, of these oscillations is not the dephasing rate of one localized region in the sample, nor is it an average of dephasing rates over the sample. Rather, it is a measure of dephasing within the localized regions *in combination* with interference among regions as a consequence of their differing Rabi nutation frequencies. Thus, when considering coherence under strong-field conditions for an inhomogeneous sample, we should replace the total homogeneous phase-slip factor with T_1/T_2^*, where T_2^* now includes the dephasing of coherence oscillations that results from different localized regions' Rabi nutation frequencies interfering with one another. This suggests that we write

$$\frac{T_1}{T_2^*} = T_1\sqrt{\gamma^2 + \left(\delta\omega_{\rm col}\left(\frac{\Theta_0}{\Theta_L} - 1\right)\right)^2}, \tag{19}$$

where $\delta\omega_{\rm col}$ is the collision shift of the 0-0 hyperfine resonance at $\zeta = 0$. (In writing Eq. (19) as a root-mean-square value, we have followed the simple approach of Danos and Geschwind for mixing homogeneous and inhomogeneous effects [34].)

To compute lineshapes under power-broadening conditions, and in particular to compute values of β that can be compared to experiment, we need some manner of relating our measured microwave powers to Rabi frequency. If we assume that the power-broadening contribution to $\Delta\nu_{1/2}$ equals γ at $P_{\mu w} = P_{\rm sat}$ [29] then we can write

$$\Omega \cong \gamma\sqrt{\frac{P_{\mu w}}{P_{\rm sat}}\left(\frac{T_1}{T_2^*}\right)^{-1}}. \tag{20}$$

Figure 15 shows two comparisons of power-broadened lineshapes: (a) under negative temperature gradient conditions and (b) under positive temperature gradient conditions. Clearly, the theory is not capable of completely capturing the lineshape asymmetry out to the wings of the line. However, in both cases near line center the agreement seems fairly good. This is especially noteworthy given the fact that T_1/T_2^* is not small, and that neither T_1/T_2^* nor Ω are free parameters. Moreover, while the wings of the lineshape are of physical interest, it is the lineshape near the peak that has technological implications (e.g., the discriminator of a vapor-cell atomic clock [35]).

Figure 16(a) compares β theoretical values with experiment. In the figure, we formed the ratio β/β_0, where β_0 is the linewidth-enhancement factor in the absence of a temperature gradient. As noted in Sec. III, β for a multilevel atom can be different from the β value for a two-level atom [25]. Consequently, taking the ratio helps account for this difference. Consistent with experiment, theory shows a roughly 60% increase in β compared to β_0 as a consequence of the temperature gradients.

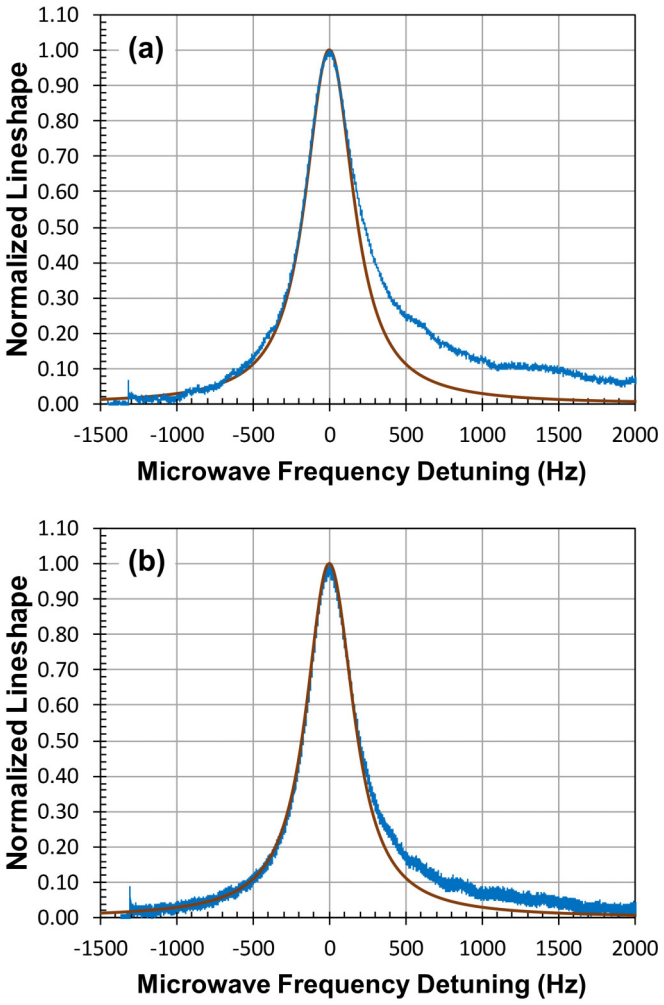

FIG. 15. (a) Comparison of theoretical and experimental lineshapes for high microwave power and high light intensity under negative temperature gradient conditions ($\Gamma_o = 5720\,{\rm s}^{-1}$, $\Omega = 80\,{\rm Hz}$, and $T_1/T_2^* = 3.52$); (b) same as (a) except for positive temperature gradient conditions ($\Gamma_o = 7180\,{\rm s}^{-1}$, $\Omega = 82\,{\rm Hz}$, and $T_1/T_2^* = 3.17$).

Figure 16(b) provides a more rigorous comparison with experiment. There, we compare theory with experiment for γ and α as functions of $P_{\mu w}$, considering one of our positive temperature-gradient experiments (i.e., $\Gamma_o = 7180\,{\rm s}^{-1}$). Given that there are no free parameters (other than A and Q, which were fixed by our low microwave power measurements), the agreement is quite reasonable. This is particularly true given the fact that our theoretical Rabi frequencies must be converted to $P_{\mu w}$ power levels via Eq. (20). Consistent with experiment, theory predicts a linear relationship between γ^2 and $P_{\mu w}$. The experimental intercept yields $\gamma = (106 \pm 3)\,{\rm Hz}$, while theory yields $\gamma = 114\,{\rm Hz}$; an 8% difference. Further, the experimental value of β is $\beta_{\rm exp} = (610 \pm 12)\,{\rm Hz/mW}^{1/2}$, while for theory we have $\beta_{\rm theo} = 451\,{\rm Hz/mW}^{1/2}$. The ratio $\beta_{\rm theo}/\beta_{\rm exp} = 0.74$, which is very respectable given the various uncertainties in the theoretical parameters. Though the theoretical values of α are in fair agreement with experiment, theory nonetheless clearly underestimates the lineshape asymmetry under power-broadening

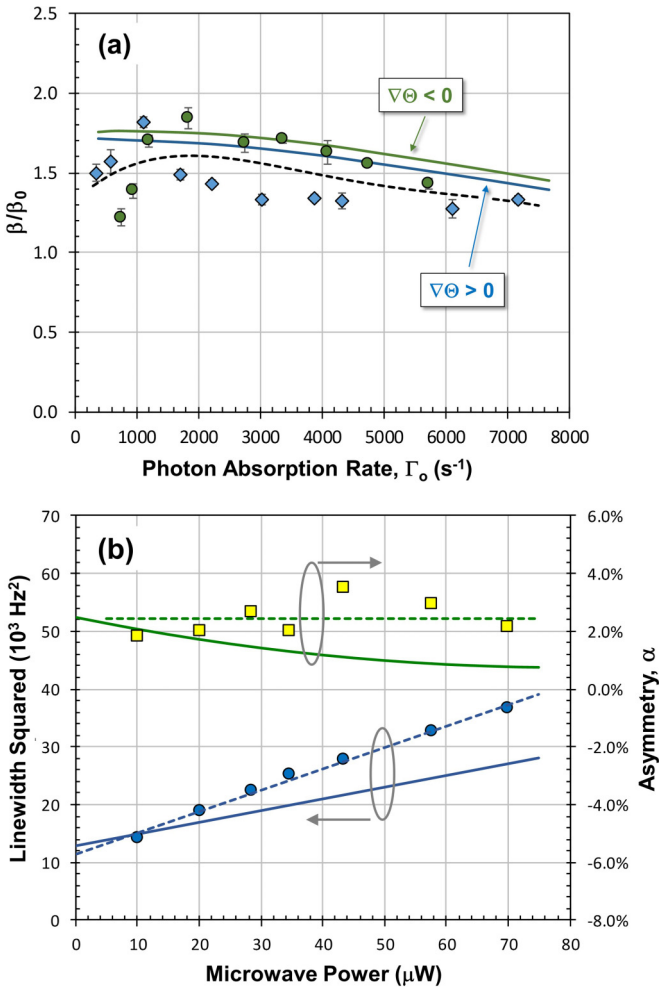

FIG. 16. (a) The linewidth enhancement factor normalized to its value under no-gradient conditions: β/β_0. Diamonds correspond to the experimental positive-gradient results, circles to the negative-gradient results, and the dashed line is a least squares fit to guide the eye treating the positive and negative-gradient results collectively. Generally, theory seems to capture the relative behavior of β as Γ_o varies. (b) For our experiment with $\Gamma_o = 7180\,\mathrm{s}^{-1}$ and a positive temperature gradient, this figure compares γ and α for theory and experiment: circles $\Rightarrow \gamma$ and squares $\Rightarrow \alpha$.

conditions. This is an aspect of theory that will require additional analysis in the future. Nevertheless it is noteworthy that theory agrees with experiment in predicting $\alpha > 0$.

V. SUMMARY

In this work, we have considered one aspect of mesoscopic vapor-phase physics as it relates to the observed 0-0 hyperfine transition in an alkali vapor: vapor temperature gradients and the collision-shift gradients they give rise to. Experimentally, we found that collision-shift gradients produce added lineshape broadening as well as lineshape asymmetry. Additionally, the linewidth-enhancement factor, β, which is a measure of how power broadening manifests itself in the observed lineshape also increased under temperature-gradient conditions. Finally, we developed a statistical theory of the lineshape that accounted for all of the observed experimental effects arising from the mesoscopic physics, and which had the added benefit of intuitive appeal.

With regard to our use of the term "mesoscopic physics" throughout this paper, one might argue that it obfuscates what is in reality a straightforward example of inhomogeneous broadening. Though we are sympathetic to that critique, we nonetheless think it misguided. In typical discussions of inhomogeneous broadening and resonant phenomena [36], dating back to the early work on the subject by Portis [37], inhomogeneous broadening has been routinely modeled via homogeneous resonance lines distributed under an envelope function, $h(\nu - \nu_o)$, with the envelope function describing the probability distribution of resonant frequencies within some space (e.g., three-dimensional physical space, velocity space for Doppler broadening, etc.). This view is certainly similar to the one taken here, where weighting functions $W_{\mathrm{op}}(\zeta)$ and $W_{\mathrm{dif}}(\zeta)$ multiplied a normalized lineshape function $L(\nu - \nu_\zeta)$. Specifically, in the standard approach to inhomogeneous broadening, we might rewrite Eq. (18) as

$$L_{\mathrm{obs}}(\nu) = \int_0^\infty h(\nu_\zeta - \nu_p) L(\nu - \nu_\zeta) d\nu_\zeta, \qquad (21)$$

where ν_p is the peak frequency for the envelope function.

The problem with Eq. (21) is that it often presumes that the parameters affecting $h(\nu_\zeta - \nu_p)$ are distinct from those affecting the lineshape function $L(\nu - \nu_\zeta)$. Though we recognize that this is not required by the definition of inhomogeneous broadening, it is nonetheless built into most models of the phenomena. In the present situation this is clearly not the case: the light intensity (i.e., $\Gamma_o(\zeta)$) clearly defines $W_{\mathrm{op}}(\zeta)$, but it can also play a role in $L(\nu - \nu_\zeta)$ through both γ_2 and T_1 (though we have not considered that here). Further, though we designed our experiment to keep the microwave field amplitude constant over the signal volume, in most cases of technological interest (e.g., atomic clocks) the atomic vapor will be housed in a microwave cavity with its concomitant mode geometry [38]. This will give rise to a spatially varying Rabi frequency, which must appear in a new weighting factor $(W_\Omega(\zeta))$ as well as the lineshape function $L(\nu - \nu_\zeta)$. Thus, when one employs the term inhomogeneous broadening, Eq. (21) implies that the only varying parameter of the homogeneous lineshape is its resonant frequency. Our use of the term mesoscopic physics is meant to better capture the notion that *all details of the homogeneous lineshape can vary across the sample:* γ_2, T_1, Ω, *and* ν_{res}.

In future work we plan to lock the microwave frequency to the peak of the observed 0-0 hyperfine resonance, and study the influence of collision-shift gradients on the measured resonant frequency. Previous research has suggested that these collision-shift gradients play a dominant role in the long-term stability of next-generation vapor-cell atomic clocks [13]. Additionally, modulating the microwave frequency at ω_m, we plan to study the dynamics of the vapor's first- and second-harmonic responses to the modulation [39]. In the present work we have been able to model the mesoscopic physics by considering (to a large extent) different regions of the vapor as distinct. However, it is not clear at present if that assumption will hold under dynamic conditions. Generally, we expect the asymmetry of the static lineshape discovered here to manifest

itself in the first-harmonic response of the vapor, S_1, to ω_m, and result in an asymmetry of S_1 when examined as a function of the microwave frequency detuning, $\nu - \nu_{\rm res}$. One question we will be interested in answering is whether or not the degree of asymmetry in S_1 follows directly from the degree of asymmetry in the static lineshape.

ACKNOWLEDGMENTS

The authors thank Ms. Kaitlin Fundell for assistance in performing the experiments. This work was funded by U.S. Air Force Space and Missile Systems Center under Contract No. FA8802-14-C-000

[1] B. S. Mathur, H. Tang, and W. Happer, Light shifts in the alkali atoms, Phys. Rev. **171**, 11 (1968).

[2] F. Levi, J. Camparo, B. Francois, C. E. Calosso, S. Micalizio, and A. Godone, Precision test of the ac Stark shift in a rubidium atomic vapor, Phys. Rev. A **93**, 023433 (2016).

[3] W. Happer, Spin exchange, past, present and future, Ann. Phys. Fr. **10**, 645 (1985).

[4] J. Vanier, C. Jacques, and C. Audoin, Effect of spin exchange on the ground-state density matrix of alkali-metal and hydrogen atoms, Phys. Rev. A **31**, 3967 (1985).

[5] N. Fortson and B. Heckel, Spontaneous Spin Polarization and Bistability in Atomic Vapors by Optical Pumping with Unpolarized Light, Phys. Rev. Lett. **59**, 1281 (1987).

[6] A. Andalkar, R. B. Warrington, M. V. Romalis, S. K. Lamoreaux, B. R. Heckel, and E. N. Fortson, Experimental and theoretical study of spontaneous spin polarization and hysteresis in cesium vapor, Phys. Rev. A **65**, 023407 (2002).

[7] R.-B. Li, L. Zhou, J. Wang, and M.-S. Zhan, Measurement of the quadratic Zeeman shift of ^{85}Rb hyperfine levels using stimulated Raman transitions, Opt. Commun. **282**, 1340 (2009).

[8] L. Weller, K. S. Kleinbach, M. A. Zentile, S. Knappe, C. S. Adams, and I. G. Hughes, Absolute absorption and dispersion of a rubidium vapour in the hyperfine Pashen-Back regime, J. Phys. B: At. Mol. Opt. Phys. **45**, 215005 (2012).

[9] A. Risley, S. Jarvis, Jr., and J. Vanier, The dependence of frequency upon microwave power of wall-coated and buffer-gas-filled gas cell Rb^{87} frequency standards, J. Appl. Phys. **51**, 4571 (1980).

[10] J. C. Camparo, R. P. Frueholz, and C. H. Volk, Inhomogeneous light shift in alkali-metal atoms, Phys. Rev. A **27**, 1914 (1983).

[11] M. H. Mittleman, Saturation broadening by inhomogeneous fields, Phys. Rev. A **39**, 69 (1989).

[12] P. J. Oreto, Y.-Y. Jau, A. B. Post, N. N. Kuzma, and W. Happer, Buffer-gas-induced shift and broadening of hyperfine resonances in alkali-metal vapors, Phys. Rev. A **69**, 042716 (2004).

[13] C. E. Calosso, A. Godone, F. Levi, and S. Micalizio, Enhanced temperature sensitivity in vapor-cell frequency standards, IEEE Trans. Ultrason. Ferroelec. Freq. Control **59**, 2646 (2012).

[14] In addition to the difference in the two regions' buffer-gas densities due to the temperature gradient, the difference in temperature implies that collisional velocities and collision-shift coefficients will also be different in the two regions. We assume these latter differences are small; hence the use of the approximately-equal sign in Eq. (1).

[15] F. Gong, Y.-Y. Jau, and W. Happer, Nonlinear Pressure Shifts of Alkali-Metal Atoms in Inert Gases, Phys. Rev. Lett. **100**, 233002 (2008).

[16] J. Camparo, The rubidium atomic clock and basic research, Phys. Today **60**(11), 33 (2007).

[17] J. Camparo and A. Hudson, Mesoscopic physics in vapor-cell atomic clocks, in *Proc. 2017 Joint Conference of the Eur. Freq. and Time Forum and IEEE Internat. Freq. Control Symp.* (IEEE Press, Piscataway, NJ, 2017), pp. 47–54.

[18] D. Kuksenkov, S. Feld, C. Wilmsen, H. Temkin, S. Swirhun, and R. Leibenguth, Linewidth and α-factor in AlGaAs/GaAs vertical cavity surface emitting lasers, Appl. Phys. Lett. **66**, 277 (1995).

[19] Taking a scan of the transmitted light as the laser was tuned across resonance, we fit the baseline of the scan (i.e., laser off-resonance) to a third-order polynomial to determine V_o at the absorption resonance frequencies.

[20] T. J. Killian, Thermionic phenomena caused by vapors of rubidium and potassium, Phys. Rev. **27**, 578 (1926).

[21] R. W. Ditchburn and J. C. Gilmore, The vapor pressures of monatomic vapors, Rev. Mod. Phys. **13**, 310 (1941).

[22] This expression for the photon absorption rate, Γ_o, is a surrogate for the actual photon absorption rate in the experiments, since κ was determined for the laser off-resonance. During the experiments, V_L was measured with the laser on-resonance, and therefore attenuated by the optically pumped vapor.

[23] J. Vanier and L.-G. Bernier, On the signal-to-noise ratio and short-term stability of passive rubidium frequency standards, IEEE Trans. Instrum. Meas. **30**, 277 (1981).

[24] J. C. Camparo and R. P. Frueholz, Linewidths of the 0-0 hyperfine transition in optically pumped alkali-metal vapors, Phys. Rev. A **31**, 1440 (1985); Saturation of the 0-0 hyperfine-transition linewidth enhancement factor in optically pumped alkali-metal vapors, *ibid.* **32**, 1888 (1985).

[25] Y. Xiao, I. Novikova, D. F. Phillips, and R. L. Walsworth, Diffusion-Induced Ramsey Narrowing, Phys. Rev. Lett. **96**, 043601 (2006).

[26] J. Vanier, R. Kunski, N. Cyr, J. Y. Savard, and M. Têtu, On hyperfine frequency shifts caused by buffer gases: Application to the optically pumped passive rubidium frequency standard, J. Appl. Phys. **53**, 5387 (1982).

[27] J. Vanier, Optical pumping as a relaxation process, Can. J. Phys. **47**, 1461 (1969).

[28] G. E. Pake, *Paramagnetic Resonance* (W. A. Benjamin, Inc., New York, 1962), Chap. 2.

[29] J. C. Camparo, The influence of diffusional relaxation on the clock signal in the laser-pumped rubidium atomic frequency standard, Aerospace Report No. TOR-2017-00316, 5 December 2016. (Mail request for report to library.mailbox@aero.org.)

[30] D. K. Walter and W. Happer, Spin-exchange broadening of atomic clock resonances, Laser Physics **12**, 1182 (2002).

[31] S. Micalizio, A. Godone, F. Levi, and J. Vanier, Spin-exchange frequency shift in alkali-metal-vapor cell frequency standards, Phys. Rev. A **73**, 033414 (2006).

[32] Since the front and back glass walls of the resonance cell were in thermal contact with the signal volume, we take the measurements at $\zeta = 0$ and $\zeta = L$ as reasonably reliable assessments of the vapor temperature at those signal-volume axial locations.

[33] P. Minguzzi, F. Strumia, and P. Violino, Temperature effects in the relaxation of optically oriented alkali vapours, Il Nuovo Cimento **46B**, 145 (1966).

[34] M. Danos and S. Geschwind, Broadening of microwave absorption lines due to wall collisions, Phys. Rev. **91**, 1159 (1953).

[35] J. Vanier and C. Audoin, *The Quantum Physics of Atomic Frequency Standards: Vol. 2* (Adam Hilger, Bristol, 1989), Chap. 7.

[36] C. H. Poole and H. A. Farach, *Relaxation in Magnetic Resonance* (Academic Press, New York, 1971), Chap. 9.

[37] A. M. Portis, Electronic structure of F centers: Saturation of the electron spin resonance, Phys. Rev. **91**, 1071 (1953).

[38] P. Tremblay, N. Cyr, and M. Têtu, Evaluation of the performance of passive rubidium frequency standards using cavity operated in mode TE011, TE111 and TE101, in *Proc. 38th Annual Frequency Control Symposium* (IEEE Press, Piscataway, NJ, 1984), pp. 406–415.

[39] J. Camparo and G. Fathi, The second-harmonic signal in vapor-cell clocks and error-signal quality: Does S_2 imply $dS_1/d\Delta$, in *Proc. 2013 Joint UFFC, EFTF and PFM Symposium* (IEEE Press, Piscataway, NJ, 2013), pp. 224–227.